

Diagrammatic Monte Carlo study of the acoustic and the BEC polaron

Jonas Vlietinck

Department of Physics and Astronomy, Ghent University, Proeftuinstraat 86, 9000 Gent, Belgium

Wim Casteels

TQC, Universiteit Antwerpen, Universiteitsplein 1, 2610 Wilrijk, Belgium

Kris Van Houcke

*Department of Physics and Astronomy, Ghent University, Proeftuinstraat 86, 9000 Gent, Belgium and
Laboratoire de Physique Statistique, Ecole Normale Supérieure, UPMC,
Université Paris Diderot, CNRS, 24 rue Lhomond, 75231 Paris Cedex 05, France*

Jacques Tempere

*TQC, Universiteit Antwerpen, Universiteitsplein 1, 2610 Wilrijk, Belgium and
Lyman Laboratory of Physics, Harvard University, Cambridge, Massachusetts 02138, USA*

Jan Ryckebusch

Department of Physics and Astronomy, Ghent University, Proeftuinstraat 86, 9000 Gent, Belgium

Jozef T. Devreese

TQC, Universiteit Antwerpen, Universiteitsplein 1, 2610 Wilrijk, Belgium

We consider two large polaron systems that are described by a Fröhlich type of Hamiltonian, namely the Bose-Einstein condensate (BEC) polaron in the continuum and the acoustic polaron in a solid. We present ground-state energies of these two systems calculated with the Diagrammatic Monte Carlo (DiagMC) method and with a Feynman all-coupling approach. The DiagMC method evaluates up to very high order a diagrammatic series for the polaron Green's function. The Feynman all-coupling approach is a variational method that has been used for a wide range of polaronic problems. For the acoustic and BEC polaron both methods provide remarkably similar non-renormalized ground-state energies that are obtained after introducing a finite momentum cutoff. For the renormalized ground-state energies of the BEC polaron, there are relatively large discrepancies between the DiagMC and the Feynman predictions. These differences can be attributed to the renormalization procedure for the contact interaction.

PACS numbers: 71.38.Fp, 02.70.Ss, 67.85.Bc

I. INTRODUCTION

By virtue of the Coulomb interaction the presence of a charge carrier in a charged lattice induces a polarization. This effect is well-known from the description of an electron or a hole in a polar or ionic semiconductor. The term polaron was coined by Landau in 1933¹ to denote the quasiparticle comprised of a charged particle coupled to a surrounding polarized lattice. For lattice-deformation sizes of the order of the lattice parameter, one refers to the system as a small or Holstein polaron^{2,3}. For lattice-deformation sizes that are large compared to the lattice parameter, the lattice can be treated as a continuum. This system is known as a large polaron for which Fröhlich proposed the model Hamiltonian⁴

$$\begin{aligned} \hat{H}_{pol} = & \sum_{\mathbf{k}} \frac{\hbar^2 \mathbf{k}^2}{2m} \hat{c}_{\mathbf{k}}^\dagger \hat{c}_{\mathbf{k}} + \sum_{\mathbf{k}} \hbar \omega(\mathbf{k}) \hat{b}_{\mathbf{k}}^\dagger \hat{b}_{\mathbf{k}} \\ & + \sum_{\mathbf{k}, \mathbf{q}} V(\mathbf{q}) \hat{c}_{\mathbf{k}+\mathbf{q}}^\dagger \hat{c}_{\mathbf{k}} (\hat{b}_{-\mathbf{q}}^\dagger + \hat{b}_{\mathbf{q}}). \end{aligned} \quad (1)$$

Here, the $\hat{c}_{\mathbf{k}}^\dagger$ ($\hat{c}_{\mathbf{k}}$) are the creation (annihilation) operators of the charge carriers with band mass m and momentum \mathbf{k} . The second term in the above Hamiltonian gives the energy of the phonons which carry the polarization. Thereby, the operator $\hat{b}_{\mathbf{k}}^\dagger$ ($\hat{b}_{\mathbf{k}}$) creates (annihilates) a phonon with wave vector \mathbf{k} and energy $\hbar \omega(\mathbf{k})$. The last term in Eq. (1) denotes the interaction between the charge carrier and the phonons. A plethora of physical phenomena can be described by the above Fröhlich type of Hamiltonian by varying the dispersion $\omega(\mathbf{k})$ and the interaction strength $V(\mathbf{q})$. Fröhlich considered the special situation of longitudinal optical (LO) phonons which are dispersionless $\omega(\mathbf{k}) = \omega_{LO}$. In the LO limit, the interaction amplitude $V(\mathbf{q})$ in Eq. (1) adopts the form

$$V_{LO}(\mathbf{q}) = -i \frac{\hbar \omega_{LO}}{q} \left(\frac{4\pi \alpha_{LO}}{\mathcal{V}} \right)^{1/2} \left(\frac{\hbar}{2m\omega_{LO}} \right)^{1/4}. \quad (2)$$

Here, \mathcal{V} is the volume of the crystal and α_{LO} the dimensionless coupling parameter:

$$\alpha_{LO} = \frac{e^2}{\hbar} \sqrt{\frac{m}{2\hbar \omega_{LO}}} \left(\frac{1}{\epsilon_\infty} - \frac{1}{\epsilon_0} \right), \quad (3)$$

with ε_∞ (ε_0) the electronic (static) dielectric constants of the crystal and e the charge of the electron. The Fröhlich polaron which is defined by the Eqs. (1)-(2) and the dispersion $\omega(\mathbf{k}) = \omega_{LO}$, has no analytical solution.

More generally, solutions to the Eq. (1) describe a quasiparticle interacting with a bath of non-interacting bosons with energies $\hbar\omega(\mathbf{k})$ through the mediation of the interaction $V(\mathbf{q})$. One example is the acoustic polaron which corresponds to the interaction of a charge carrier with acoustic phonons⁵. Another example is the BEC polaron consisting of an impurity atom interacting with the Bogoliubov excitations of an atomic Bose-Einstein condensate (BEC)⁶⁻⁸. Other examples are an electron on a helium film (“ripplopolaron”)⁹⁻¹¹ and a charge carrier in a piezoelectric semiconductor (“piezopolaron”)¹².

Due to the relative simplicity of the model Hamiltonian of Eq. (1) it is an ideal testing ground for conducting comparative studies with various many-body techniques (see for example Refs.^{13,14} for an overview). The weak coupling regime (small α_{LO}) was described by Fröhlich with second-order perturbation theory⁴ which is equivalent to the Lee-Low-Pines scheme using a canonical transformation¹⁵. For the strong coupling regime (large α_{LO}) Landau and Pekar developed a variational technique which predicts the formation of a bound state of the charge carrier in his self-induced potential^{16,17}. Feynman developed a superior all-coupling approach^{18,19} which captures all the coupling regimes.

A numerical solution of the Fröhlich Hamiltonian of Eq. (1) with the interaction of Eq. (2) has been proposed in Refs.^{20,21}. Thereby, a series expansion for the polaron Green’s function was evaluated with the aid of a Diagrammatic Monte Carlo (DiagMC) method. The method is “exact” in the sense that the series expansion is convergent and sign-definite and therefore it can be stochastically evaluated with a controllable error. The polaron’s energy is extracted from the asymptotic behavior of its Green’s function.

Polaron systems are ideal for comparative studies of many-body techniques. Examples of such studies for the Fermi polaron are reported in Refs.²²⁻²⁴. For the Fermi polaron, a comparison has been made between the DiagMC method and the variational technique which includes a limited number of particle-hole excitations. It was demonstrated that a variational one particle-hole calculation is already a good approximation, even for strong interactions between the impurity and the particles in the Fermi sea^{23,24}. Recently a comparative study of the neutron polaron has been conducted with quantum Monte Carlo and effective field theories²⁵. For the ground-state energy of the Fröhlich polaron of Eqs. (1) and (2) it has been shown in Ref.²⁰ that Feynman’s approach reproduces the DiagMC results to a remarkable accuracy. We have reproduced those numerical results. As can be appreciated from Fig. 1 the deviations between the variational Feynman and DiagMC predictions for the ground-state energies of the Fröhlich polaron, are of the order of a few percent, even for the large cou-

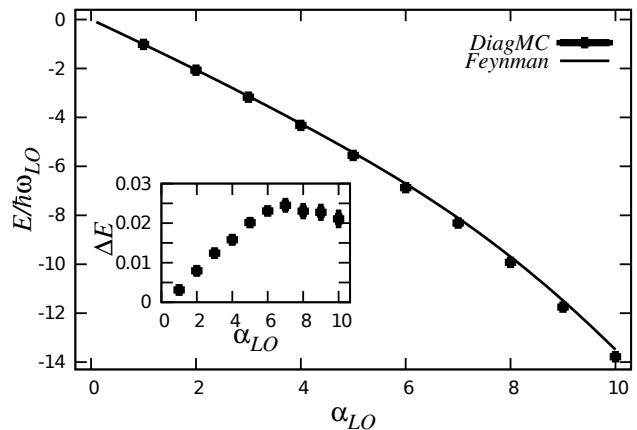


FIG. 1. Ground-state energies for the Fröhlich polaron are shown as a function of the coupling strength α_{LO} of Eq. (3). The inset shows the relative difference $\Delta E = \frac{E^{MC} - E^F}{E^{MC}}$, with E^F (E^{MC}) the computed energy from the Feynman (DiagMC) approach.

pling strengths. It is not clear, however, how accurate the Feynman technique is for polaron systems described by a Hamiltonian of the type of Eq. (1) with alternate dispersions $\omega(\mathbf{k})$ and interaction amplitudes $V(\mathbf{q})$. Indeed, Feynman’s approach is based on a variational action functional that models the coupling to the phonons by a single phononic degree of freedom with a variationally determined mass and harmonic coupling to the electron. This is a rather natural choice for LO phonons, which are dispersionless. However, it seems intuitively less suitable in situations that the phonons’ energies cover a finite range of values. Thornber²⁶ has argued that in those situations, Feynman’s model is unlikely to yield accurate results for the system’s dynamical properties, but that the system’s ground-state energy can still be captured accurately. To our knowledge, this assertion has not yet been sufficiently confirmed. In order to remedy this situation, in this work we compare polaron ground-state energies calculated with the Feynman variational approach against DiagMC results. This will allow us to test the robustness of the Feynman approach. The two prototypical polaron problems considered in this work are the BEC polaron and the acoustic polaron. These problems have been selected because they highlight complementary aspects. The effect of broadening the range of phonon energies is captured by the acoustic polaron. The BEC polaron problem allows one to additionally cover the issues related to renormalizing $V(\mathbf{q})$.

The structure of this manuscript is as follows. In Sec. II the Hamiltonians for the BEC and acoustic polaron are introduced. In Sects. III A and III B the adopted many-body methods for obtaining the ground-state energies of those Hamiltonians are sketched. Results of the two techniques for the ground-state energies of the BEC and acoustic polaron are contained in Sec. IV.

II. LARGE POLARON MODELS

A. BEC polaron

The Hamiltonian of an impurity immersed in a bath of interacting bosons⁸ is given by a sum of two terms $\hat{H} = \hat{H}_B + \hat{H}_I$ with,

$$\begin{aligned}\hat{H}_B &= \sum_{\mathbf{k}} \epsilon_{\mathbf{k}} \hat{a}_{\mathbf{k}}^\dagger \hat{a}_{\mathbf{k}} + \frac{1}{2\mathcal{V}} \sum_{\mathbf{k}, \mathbf{k}', \mathbf{q}} V_{BB}(\mathbf{q}) \hat{a}_{\mathbf{k}'-\mathbf{q}}^\dagger \hat{a}_{\mathbf{k}+\mathbf{q}}^\dagger \hat{a}_{\mathbf{k}} \hat{a}_{\mathbf{k}'} , \\ \hat{H}_I &= \sum_{\mathbf{k}} \frac{\hbar^2 \mathbf{k}^2}{2m_I} \hat{c}_{\mathbf{k}}^\dagger \hat{c}_{\mathbf{k}} + \frac{1}{\mathcal{V}} \sum_{\mathbf{k}, \mathbf{k}', \mathbf{q}} V_{IB}(\mathbf{q}) \hat{c}_{\mathbf{k}+\mathbf{q}}^\dagger \hat{c}_{\mathbf{k}} \hat{a}_{\mathbf{k}'-\mathbf{q}}^\dagger \hat{a}_{\mathbf{k}'} .\end{aligned}\quad (4)$$

The operators $\hat{a}_{\mathbf{k}}^\dagger (\hat{a}_{\mathbf{k}})$ create (annihilate) bosons with momentum \mathbf{k} , mass m and energy $\epsilon_{\mathbf{k}} = \hbar^2 \mathbf{k}^2 / 2m$. Further, \mathcal{V} is the volume of the system. The operators $\hat{c}_{\mathbf{k}}^\dagger (\hat{c}_{\mathbf{k}})$ create (annihilate) the impurity with momentum \mathbf{k} and mass m_I . The boson-boson and impurity-boson interactions in momentum space are $V_{BB}(\mathbf{q})$ and $V_{IB}(\mathbf{q})$. These potentials are replaced by the pseudopotentials g_{BB} and g_{IB} . These constants are chosen such that the two-body scattering properties in vacuum are correctly reproduced. The sum of all vacuum ladder diagrams, given by the T -matrix, represents all possible ways in which two particles can scatter in vacuum. For zero momentum and frequency the T -matrix is given by $T(0)$:

$$T(0) = g_{IB} - g_{IB} \sum_{\mathbf{k}} \frac{2m_r}{\hbar^2 k^2} T(0) , \quad (5)$$

with $m_r = (1/m_I + 1/m)^{-1}$ the reduced mass. For low-energy collisions the first-order Born approximation can be applied to model the boson-boson and boson-impurity collisions. As a result, $g_{IB} = \frac{2\pi a_{IB} \hbar^2}{m_r}$, with a_{IB} the boson-impurity scattering length and $g_{BB} = \frac{4\pi a_{BB} \hbar^2}{m}$, with a_{BB} the boson-boson scattering length.

In the Bogoliubov approximation²⁷, the Hamiltonian \hat{H}_B of Eq. (4) is written in the diagonal form

$$\hat{H}_B \approx E_0 + \sum_{\mathbf{k} \neq 0} \hbar \omega(\mathbf{k}) \hat{b}_{\mathbf{k}}^\dagger \hat{b}_{\mathbf{k}} , \quad (6)$$

where the operators $\hat{b}_{\mathbf{k}}^\dagger (\hat{b}_{\mathbf{k}})$ create (annihilate) Bogoliubov quasi-particles. The quasi-particle vacuum energy is

$$E_0 = \frac{\mathcal{V}}{2} n^2 g_{BB} + \frac{1}{2} \sum_{\mathbf{k} \neq 0} \left(\hbar \omega(\mathbf{k}) - \epsilon_{\mathbf{k}} - n_0 g_{BB} \right) , \quad (7)$$

with $n = N/\mathcal{V}$ the total density and $n_0 = N_0/\mathcal{V}$ the density of the condensed bosons. The average total particle number $N = \langle \hat{N} \rangle$ is fixed, with

$$\hat{N} = N_0 + \sum_{\mathbf{k} \neq 0} \hat{a}_{\mathbf{k}}^\dagger \hat{a}_{\mathbf{k}} , \quad (8)$$

and N_0 the number of bosons in the condensate. The collective Bogoliubov excitations obey the dispersion relation

$$\hbar \omega(\mathbf{k}) = \sqrt{(\epsilon_{\mathbf{k}} + n_0 g_{BB})^2 - (n_0 g_{BB})^2} . \quad (9)$$

At long wavelengths, the spectrum becomes $\omega(\mathbf{k}) = |\mathbf{k}|c$, which is characteristic of a sound wave with velocity $c = \sqrt{n_0 g_{BB}/m}$. The excitation spectrum is conveniently written in the form

$$\omega(\mathbf{k}) = kc \sqrt{1 + \frac{(k\xi)^2}{2}} , \quad (10)$$

with $k = |\mathbf{k}|$ and $\xi = 1/\sqrt{2mn_0 g_{BB}}$ the healing length of the Bose condensate.

Application of the Bogoliubov transformation to the impurity part \hat{H}_I of Eq. (4) gives⁶⁻⁸

$$\begin{aligned}\hat{H}_I &\approx \sum_{\mathbf{k}} \frac{\hbar^2 \mathbf{k}^2}{2m_I} \hat{c}_{\mathbf{k}}^\dagger \hat{c}_{\mathbf{k}} + n_0 g_{IB} \\ &+ \sum_{\mathbf{q} \neq 0, \mathbf{k}} V_{BP}(\mathbf{q}) \hat{c}_{\mathbf{k}+\mathbf{q}}^\dagger \hat{c}_{\mathbf{k}} (\hat{b}_{-\mathbf{q}}^\dagger + \hat{b}_{\mathbf{q}}) ,\end{aligned}\quad (11)$$

in which we have defined

$$\begin{aligned}V_{BP}(\mathbf{q}) &= \frac{g_{IB}}{\mathcal{V}} \sqrt{\frac{N_0 \epsilon_{\mathbf{q}}}{\omega(\mathbf{q})}} \\ &= \frac{g_{IB} \sqrt{N_0}}{\mathcal{V}} \left(\frac{(\xi q)^2}{(\xi q)^2 + 2} \right)^{1/4} .\end{aligned}\quad (12)$$

For $g_{IB} = \frac{2\pi a_{IB} \hbar^2}{m_r}$ a dimensionless coupling constant α_{IB} can be defined⁸

$$\alpha_{IB} = \frac{a_{IB}^2}{a_{BB} \xi} . \quad (13)$$

The final expression for the Hamiltonian for the BEC polaron is given by

$$\begin{aligned}\hat{H}_{BP} &= E_0 + n_0 g_{IB} + \sum_{\mathbf{k}} \frac{\hbar^2 \mathbf{k}^2}{2m_I} \hat{c}_{\mathbf{k}}^\dagger \hat{c}_{\mathbf{k}} + \sum_{\mathbf{k} \neq 0} \hbar \omega(\mathbf{k}) \hat{b}_{\mathbf{k}}^\dagger \hat{b}_{\mathbf{k}} \\ &+ \sum_{\mathbf{q} \neq 0, \mathbf{k}} V_{BP}(\mathbf{q}) \hat{c}_{\mathbf{k}+\mathbf{q}}^\dagger \hat{c}_{\mathbf{k}} (\hat{b}_{-\mathbf{q}}^\dagger + \hat{b}_{\mathbf{q}}) .\end{aligned}\quad (14)$$

Obviously, the \hat{H}_{BP} has the format of a Fröhlich-type of Hamiltonian defined in Eq. (1). When presenting numerical results for the BEC polaron, lengths will be expressed in units of ξ , energies in units of $\frac{\hbar^2}{m\xi^2}$ and phonon wave vectors in units of $1/\xi$. In this way, all quoted variables are dimensionless. In the numerical calculations, we consider an ⁶Li impurity in a Na condensate for which $m_I/m_B = 0.263158$ ⁸.

B. Acoustic polaron

In a crystal with two or more atoms per primitive cell, the dispersion relation $\omega(\mathbf{k})$ for the phonons develops acoustic as well as optical branches. The acoustic polaron comprises a charge carrier interacting with the longitudinal acoustic phonons and can be described by the Fröhlich type of Hamiltonian of Eq. (1) with the dispersion $\omega(\mathbf{k}) = sk$, with s the sound velocity⁵. For the acoustic polaron, the interaction $V_{AC}(\mathbf{q})$ in the Fröhlich Hamiltonian adopts the form⁵:

$$V_{AC}(\mathbf{q}) = \left(\frac{4\pi\alpha_{AC}}{\mathcal{V}} \right)^{1/2} \frac{\hbar^2}{m} \sqrt{q}, \quad (15)$$

with \mathcal{V} the volume of the crystal and α_{AC} a dimensionless coupling parameter. When discussing results concerning the acoustic polaron, lengths will be expressed in units of $\hbar/(ms)$, energies in units of ms^2 and phonon wave vectors in units of ms/\hbar . The summations over the phonon momenta $|\mathbf{k}|$ have a natural cut-off at the boundary k_0 of the first Brillouin zone. At strong coupling, the Feynman approach to the acoustic polaron predicts the emergence of a self-induced binding potential for the impurity (“self-trapped state”). For a system with both Fröhlich and acoustic phonons, the Feynman approach predicts that the dominant mechanism for this transition is the interaction with the acoustic phonons²⁸. Only considering the acoustic phonons results in a transition of the first order for $k_0 > 18$ and a critical point at $k_0 \approx 18$ and $\alpha_{AC} \approx 0.151$ ⁵. This transition was also predicted by the path integral Monte Carlo method²⁹.

III. NUMERICAL METHODS

A. Feynman variational path integral

The Feynman approach is based on the Jensen-Feynman inequality for the free energy \mathcal{F} of a system with action \mathcal{S} ¹⁹:

$$\mathcal{F} \leq \mathcal{F}_0 + \frac{1}{\hbar\beta} \langle \mathcal{S} - \mathcal{S}_0 \rangle_{\mathcal{S}_0}. \quad (16)$$

Here, \mathcal{F}_0 is the free energy of a trial system with action \mathcal{S}_0 , $\langle \dots \rangle_{\mathcal{S}_0}$ denotes the expectation value with respect to the trial system and $\beta = (k_B T)^{-1}$ is the inverse temperature. Feynman proposed a variational trial system of a charge carrier harmonically coupled with spring frequency W to a fictitious particle with mass M . For $T = 0$ the Jensen-Feynman inequality of Eq. (16) applied to this system produces an upper bound E_p^F for the pola-

ronic ground-state energy^{18,19}:

$$E_p \leq \frac{3\hbar\Omega}{4} \frac{\left(\sqrt{(1 + M/m_I)} - 1 \right)^2}{1 + M/m_I} + \sum_{\mathbf{k}} \frac{|V_{\mathbf{k}}|^2}{\hbar} \int_0^\infty du \mathcal{D}(\mathbf{k}, u) \mathcal{M}(\mathbf{k}, u), \quad (17)$$

with $\Omega = W\sqrt{1 + M/m}$. The function $\mathcal{D}(\mathbf{k}, u)$ is the phonon Green’s function in momentum-imaginary-time representation (\mathbf{k}, τ)

$$\mathcal{D}(\mathbf{k}, \tau) = -\theta(\tau) \exp[-\omega(\mathbf{k})\tau], \quad (18)$$

where $\theta(\tau)$ is the Heaviside function. The memory function $\mathcal{M}(\mathbf{k}, u)$ is:

$$\mathcal{M}(\mathbf{k}, u) = \exp \left[-\frac{\hbar k^2}{2(m_I + M)} \times \left(u + \frac{M}{m_I} \frac{1 - \exp[-\Omega u]}{\Omega} \right) \right]. \quad (19)$$

The u -integral in Eq. (17) is of the following form:

$$\int_0^\infty du \exp[-au + be^{-u}] = -(-b)^{-a} \Gamma(a, -b, 0), \quad (20)$$

with $\Gamma(a, z_0, z_1) = \int_{z_0}^{z_1} t^{a-1} e^{-t} dt$ the generalized incomplete gamma function. The parameters M and Ω are used to minimize the upper bound for the ground state energy of Eq. (17). This approach captures the different coupling regimes.

B. One-body propagator and DiagMC

The Green’s function of the polaron in the (\mathbf{k}, τ) representation is defined as:

$$G(\mathbf{k}, \tau) = -\theta(\tau) \langle \text{vac} | \hat{c}_{\mathbf{k}}(\tau) \hat{c}_{\mathbf{k}}^\dagger(0) | \text{vac} \rangle, \quad (21)$$

with

$$\hat{c}_{\mathbf{k}}(\tau) = e^{\hat{H}\tau} \hat{c}_{\mathbf{k}} e^{-\hat{H}\tau}, \quad (22)$$

the annihilation operator in the Heisenberg representation and $|\text{vac}\rangle$ the vacuum state. The BEC polaron Hamiltonian \hat{H}_{BP} of Eq. (14) contains a vacuum energy $E_0 + n_0 g_{IB}$ which we choose as the zero of the energy scale. Accordingly, $\hat{H}_{BP} |\text{vac}\rangle = 0$. We define $\{|\nu(\mathbf{k})\rangle\}$ as those eigenfunctions of \hat{H}_{BP} with energy eigenvalue $E_\nu(\mathbf{k})$ and with one impurity with momentum \mathbf{k} . Inserting a complete set of eigenstates in Eq. (21) gives

$$G(\mathbf{k}, \tau) = -\theta(\tau) \sum_{\nu} |\langle \nu(\mathbf{k}) | \hat{c}_{\mathbf{k}}^\dagger | \text{vac} \rangle|^2 e^{-E_\nu(\mathbf{k})\tau}. \quad (23)$$

Under the conditions that the polaron is a stable quasiparticle in the ground state (in the sense that it appears

as a δ -function peak in the spectral function), one can extract its energy $E_p(\mathbf{k})$ and Z -factor Z_0 by studying the long imaginary time behavior of the polaron's Green's function:

$$G(\mathbf{k}, \tau) \xrightarrow{\tau \rightarrow +\infty} -Z_0(\mathbf{k}) e^{-(E_p(\mathbf{k}) - \mu)\tau}, \quad (24)$$

where the parameter μ is introduced to render a descending exponential tail and

$$Z_0(\mathbf{k}) = |\langle \Psi(\mathbf{k}) | \hat{c}_{\mathbf{k}}^\dagger | \text{vac} \rangle|^2, \quad (25)$$

with $\Psi(\mathbf{k})$ the fully interacting ground state. The asymptotic behavior of Eq. (24) is associated with a pole singularity for the Green's function in imaginary-frequency representation. For $(E_p(\mathbf{k}) - \mu) > 0$ one has

$$\begin{aligned} G(\mathbf{k}, \omega) &= \int_0^{+\infty} d\tau e^{i\omega\tau} G(\mathbf{k}, \tau) \\ &= \frac{Z_0(\mathbf{k})}{i\omega + \mu - E_p(\mathbf{k})} + \text{regular part}. \end{aligned} \quad (26)$$

The one-body self-energy $\Sigma(\mathbf{k}, \omega)$ is related to the Green's function by means of the Dyson equation

$$G(\mathbf{k}, \omega) = \frac{1}{\frac{1}{G^0(\mathbf{k}, \omega)} - \Sigma(\mathbf{k}, \omega)}, \quad (27)$$

with $G^0(\mathbf{k}, \omega)$ the free impurity Green's function. Since the Eqs. (26) and (27) possess the same pole structure, the following expression for the polaronic ground-state energy $E_p = E_p(\mathbf{k} = \mathbf{0})$ can be obtained²⁰:

$$E_p = \int_0^\infty d\tau \Sigma(\tau) e^{(E_p - \mu)\tau}, \quad (28)$$

with $\Sigma(\tau) = \Sigma(\mathbf{0}, \tau)$. Calculating the Green's function boils down to summing a series of Feynman diagrams over all topologies and orders, thereby integrating over all internal variables (like momentum and imaginary time). It is shown in²⁰ that DiagMC is very suitable to accurately compute the Green's function through a series expansion. We consider irreducible diagrams (an example is shown in Fig. 2) and evaluate a large number of diagrams D in order to numerically compute the $\Sigma(\mathbf{p}, \tau)$

$$\begin{aligned} \Sigma(\mathbf{p}, \tau) &= \sum_{n=0}^\infty \sum_{\xi_n} \sum_{\mathbf{q}_i=1, \dots, n} \int d\tau_1 \dots d\tau_i \dots d\tau_n \\ &\times D(\xi_n, \mathbf{p}, \tau, \tau_1, \dots, \tau_i, \dots, \tau_n, \mathbf{q}_1, \dots, \mathbf{q}_i, \dots, \mathbf{q}_n), \end{aligned} \quad (29)$$

where ξ_n represents the topology, n the diagram order, \mathbf{q}_i is the internal momentum and τ_i is the imaginary time. The DiagMC technique allows one to sample over all topologies, all orders and all values of the internal variables.

In Fig. 2 some Feynman diagrams for $\Sigma(\tau)$ are shown. The algebraic expression for these diagrams is given in terms of free propagators and interaction vertices:

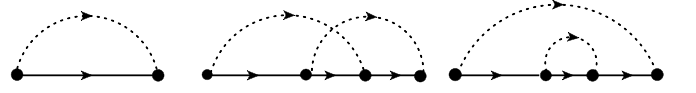


FIG. 2. Irreducible diagrams for the polaron's self-energy $\Sigma(\tau)$. Imaginary time runs from left to right. A solid line represents a free-impurity propagator and a dashed line stands for an elementary excitation. The interaction vertices are denoted by dots.

- (i) The free-impurity propagator in imaginary time is determined by

$$G^{(0)}(\mathbf{k}, \tau) = -\theta(\tau) e^{-(\epsilon_k - \mu)\tau}. \quad (30)$$

- (ii) The propagator for an elementary phonon excitation, either of the Bogoliubov type for the BEC polaron, or acoustic phonons for the acoustic polaron is defined in Eq. (18).
- (iii) A vertex factor $V(\mathbf{q})$ whenever an elementary excitation carrying momentum \mathbf{q} is created or annihilated.

The diagram order is defined by the number of elementary excitations.

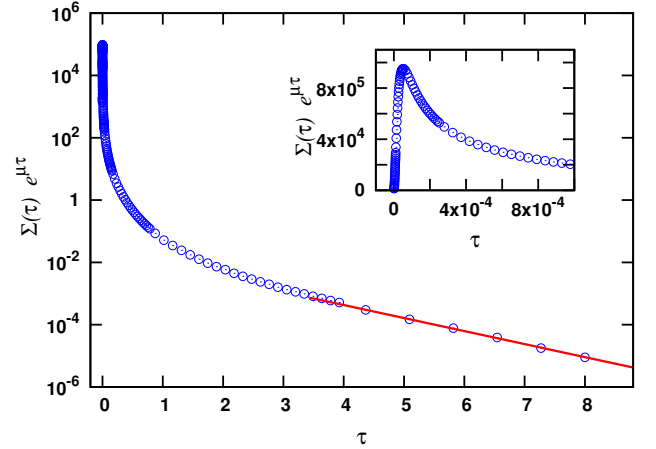


FIG. 3. (Color online) The one-body self-energy $\Sigma(\tau)e^{\mu\tau}$ for $\mu = -2$ for the BEC polaron plotted as a function of imaginary time τ . Results are obtained for $\alpha_{IB} = 5$ and $q_c = 200$ and exclude the first-order contribution to $\Sigma(\tau)e^{\mu\tau}$ which can be easily computed analytically. The inset shows $\Sigma(\tau)e^{\mu\tau}$ for small imaginary times.

IV. RESULTS AND DISCUSSION

A. BEC polaron

For the Fröhlich polaron for which the ground-state energies are displayed in Fig. 1, the one-body self-energy $\Sigma(\tau)$ can be computed by means of the procedure

sketched in Sec. III B. For the BEC polaron, on the other hand, one encounters ultraviolet divergences when evaluating $\Sigma(\tau)$ and its energy cannot be extracted. Renormalization/regularization of the impurity-boson pseudopotential is required to obtain physically relevant results for the energies. As a first step in the renormalization procedure, we introduce a momentum cutoff q_c upon replacing the momentum summations in Eq. (14) by integrals:

$$\sum_{\mathbf{k}} \rightarrow \frac{\mathcal{V}}{(2\pi)^3} \int_{|\mathbf{k}| < q_c} d\mathbf{k}. \quad (31)$$

This allows us to calculate $\Sigma(\tau)$ and the accompanying ground-state energy E_p^{MC} . From now on we will make the distinction between the polaron energy calculated by DiagMC (E_p^{MC}) and calculated by the Feynman approach (E_p^F). Obviously, $E_p^{MC,F}$ depends on q_c and in order to stress this dependence we use the notation $E_p^{MC,F}(q_c)$. In Fig. 3 we show an example of the time dependence of the one-body self-energy $\Sigma(\tau)$ for the BEC polaron for $q_c = 200$. As can be noticed, after introducing a momentum cutoff q_c , the τ dependence is well behaved and the asymptotic regime of $\Sigma(\tau)$ can be identified. The $\sum_{n=0}^{\infty}$ in Eq. (29) implies a summation over an infinite number of diagram orders. In practice, we set a cutoff N_{\max} for n in evaluating $\Sigma(\tau)$. For each N_{\max} we can find a corresponding imaginary time τ_{\max} for which $\Sigma(\tau)$ converges. Upon increasing N_{\max} we can choose a larger value for τ_{\max} . An optimal N_{\max} is reached when we can find a τ_{\max} in the asymptotic regime that allows us to fit the tail of $\Sigma(\tau)$. In this way we make an extrapolation for $\tau \rightarrow \infty$ which determines the value N_{\max} . Typical values of N_{\max} are of the order 10^4 for large values of α_{IB} . With the aid of the Eq. (28), $E_p^{MC}(q_c)$ can be extracted from the computed $\Sigma(\tau)$. The error on $E_p^{MC}(q_c)$ contains a statistical error and a systematic error stemming from the fitting procedure. As can be appreciated from Fig. 3, the grid in imaginary time has to be chosen carefully, since the short-time behavior of $\Sigma(\tau)$ is strongly peaked. The $\Sigma(p, \tau)$ for these short times delivers a large contribution to the energy.

In Fig. 4, results for the non-renormalized energies $E_p^F(q_c)$ and $E_p^{MC}(q_c)$ are presented as a function of the dimensionless coupling parameter α_{IB} defined in Eq. (13). The α_{IB} and q_c dependence of the DiagMC energies is remarkably similar to those of the Feynman energies. We observe that $E_p^{MC}(q_c)$ lies a few percent below $E_p^F(q_c)$ for all combinations of α_{IB} and q_c considered.

In Ref.⁸ a renormalization procedure to eliminate the q_c dependence of the computed polaron energy is outlined. When determining the T -matrix of Eq. (5) up to second order, the following relation between the scattering length a_{IB} and the coupling strength g_{IB} is obtained:

$$\frac{2\pi a_{IB} \hbar^2}{m_r} = g_{IB} - \frac{g_{IB}^2}{(2\pi)^3} \int_{|\mathbf{q}| < q_c} d\mathbf{q} \frac{2m_r}{\hbar^2 q^2}. \quad (32)$$

Using this expression, the $n_0 g_{IB}$ term in Eq. (14) can

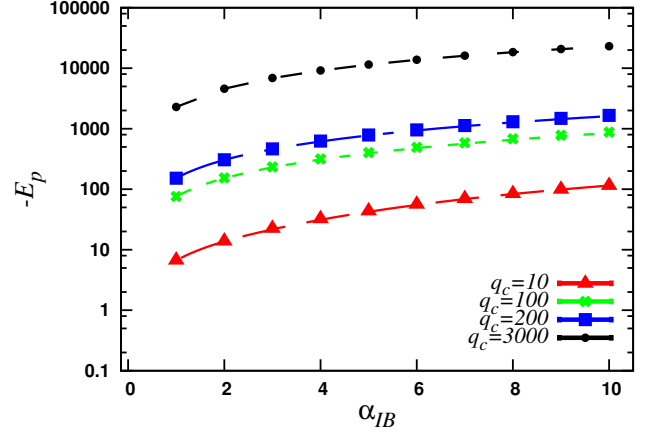


FIG. 4. (Color online) The non-renormalized BEC-polaron energy E_p as a function of the coupling strength α_{IB} as computed with the DiagMC (symbols) and with the Feynman (lines) approaches. Results are shown for four values of the cutoff momentum.

be replaced by :

$$n_0 g_{IB} \rightarrow \frac{2\pi a_{IB} n_0 \hbar^2}{m_r} + E_{\text{ren}}(q_c), \quad (33)$$

whereby we have defined $E_{\text{ren}}(q_c)$:

$$E_{\text{ren}}(q_c) = \frac{n_0 g_{IB}^2}{(2\pi)^3} \int_{|\mathbf{q}| < q_c} d\mathbf{q} \frac{2m_r}{\hbar^2 q^2}. \quad (34)$$

This renormalization procedure was developed in the context of the Feynman approach⁸. The same procedure can also be applied in the DiagMC framework. In both frameworks, the renormalized polaron ground-state energy can be found by evaluating the sum

$$E_p^{MC,F} = E_p^{MC,F}(q_c \rightarrow \infty) + E_{\text{ren}}(q_c \rightarrow \infty). \quad (35)$$

In order to illustrate the convergence of the Eq. (35) in both approaches, in Fig. 5 the energies $[E_p^{MC}(q_c) + E_{\text{ren}}(q_c)]$ and $[E_p^F(q_c) + E_{\text{ren}}(q_c)]$ are plotted as a function of q_c for a representative value $\alpha_{IB} = 3$ of the coupling strength. We notice that the DiagMC and the Feynman approach display an analogous q_c dependence. Convergence is reached for $q_c \gtrsim 3000$. Fig. 6 shows that the Feynman path-integral predictions for the BEC-polaron ground-state energies overshoot the DiagMC ones. The relative difference between the two predictions increases with growing values of q_c . The very good agreement between the two methods that was found in Fig. 4 for the non-renormalized energies, is no longer observed for the renormalized energies. Indeed, the latter are obtained with Eq. (35), which amounts to subtracting two numbers of almost equal magnitude. Accordingly, the final result for the renormalized BEC-polaron ground-state energy is highly sensitive to the adopted many-body technique and renormalization procedure. Fig. 7 illustrates

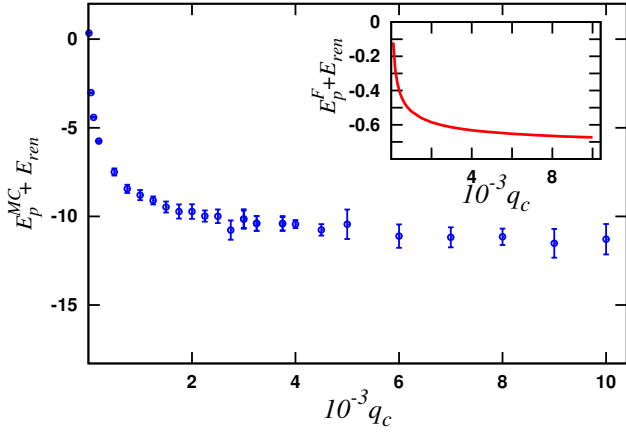


FIG. 5. (Color online) The renormalized BEC-polaron energies $[E_p^{MC}(q_c) + E_{ren}(q_c)]$ at $\alpha_{IB} = 3$ are given as a function of the momentum cutoff q_c . The inset figure shows $[E_p^F(q_c) + E_{ren}(q_c)]$ as a function of q_c .

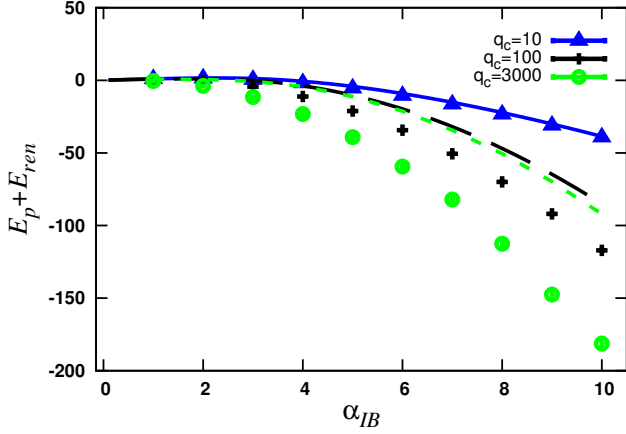


FIG. 6. (Color online) The renormalized BEC-polaron energies $[E_p(q_c) + E_{ren}(q_c)]$ as a function of α_{IB} for different values of the momentum cutoff q_c . Lines are the Feynman path-integral and symbols are the DiagMC results.

that for small α_{IB} both methods reproduce the result from second-order perturbation theory.

The DiagMC method samples diagrams according to their weight and it can be recorded how many times a specific diagram is sampled. In this way, one can identify those diagrams with the largest weight in the self-energy $\Sigma(\tau)$. At fixed diagram order, we have observed that the number of first-order subdiagrams—the definition of which is explained in the caption of Fig. 8—plays a crucial role in the weight of the diagram. Our studies indicate that for $q_c > 50$ the most important diagram is the one with the highest number of first-order subdiagrams. We have considered many combinations of α_{IB} and q_c and could draw this conclusions in all those situations. The dominance of this diagram becomes more explicit with

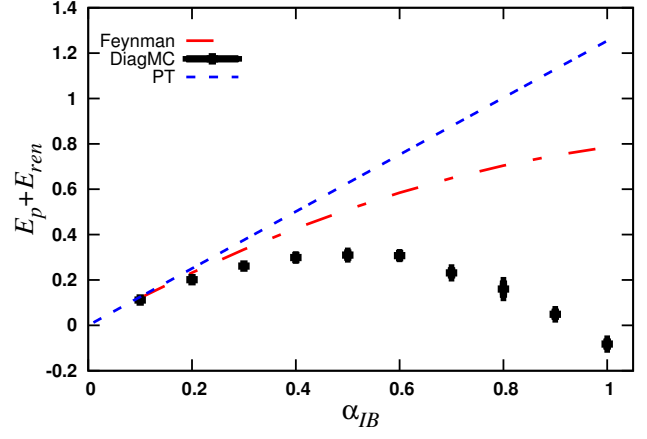


FIG. 7. (Color online) The renormalized BEC-polaron energies $[E_p(q_c) + E_{ren}(q_c)]$ at small values of α_{IB} at $q_c = 2000$. The dot-dashed line is the Feynman path-integral result, symbols represent the DiagMC results, while the short dashed line is the prediction from second-order perturbation theory (PT).

increasing values of q_c .

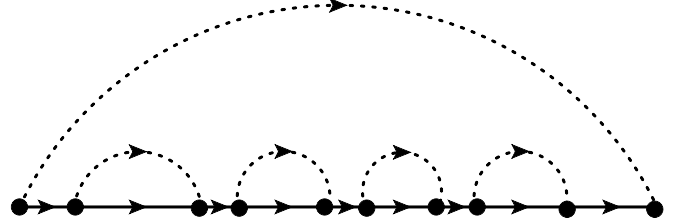


FIG. 8. A diagram of order five for the one-body self-energy. Line conventions as in Fig. 2. Imaginary time runs from left to right. A first-order subdiagram occurs whenever a first-order diagram drops out from the full diagram by cutting the solid line at two selected times. For example, the considered diagram contains four first-order subdiagrams.

B. Acoustic polaron

We now discuss the numerical results for the ground-state energy of the acoustic polaron introduced in Sec. II B. In Figs. 9 and 10 we show a selection of the predictions E_p^F from the Feynman upper-bound method of Eq. (17) together with the DiagMC results E_p^{MC} which are computed with the aid of Eq. (28). For $k_0 = 10$ and $k_0 = 50$ an excellent agreement between E_p^F and E_p^{MC} is found. From the relative difference $\Delta E = \frac{E_p^{MC} - E_p^F}{E_p^{MC}}$, a value α_{AC} can be found where ΔE is largest in the considered region of α_{AC} . For $k_0 = 10$ we find $\alpha_{AC}^{k_0=10} = 0.28 \pm 0.04$ and for $k_0 = 50$, $\alpha_{AC}^{k_0=50} = 0.52 \pm 0.01$. For $\alpha < \alpha_c$, ΔE increases with α_{AC} and for $\alpha > \alpha_c$ ΔE decreases with increasing α_{AC} . We remark that $\alpha_c^{k_0=10}$

and $\alpha_c^{k_0=50}$ coincides with the coupling strength for the transition²⁸ as computed with the Feynman approach.

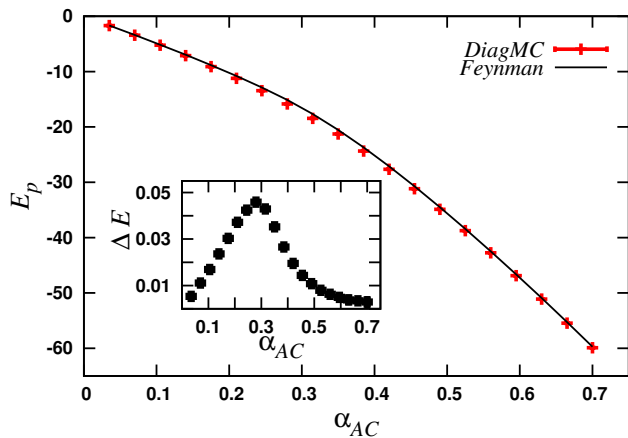


FIG. 9. Non-renormalized ground-state energies E_p^F and E_p^{MC} for the acoustic polaron as a function of α_{AC} for $k_0 = 10$. The inset shows $\Delta E = \frac{E_p^{MC} - E_p^F}{E_p^{MC}}$ as a function of α_{AC} .

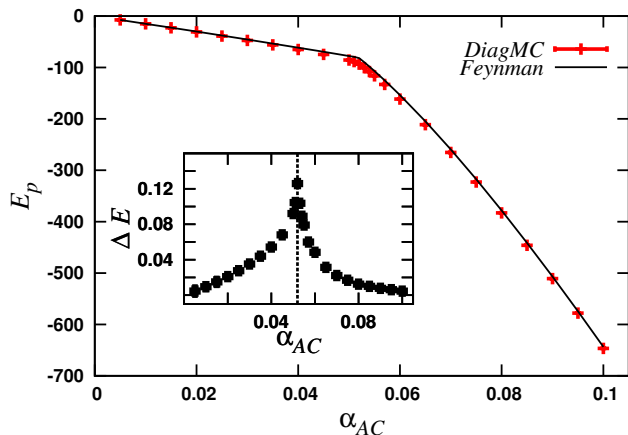


FIG. 10. As in Fig. 9 but for $k_0 = 50$. The vertical dashed line denotes the coupling strength $\alpha_{AC} = 0.052$ corresponding with the transition as computed in Ref.⁵.

From a detailed analysis of the DiagMC results for $k_0 = 50$ we find that the class of diagrams of the type sketched in Fig. 8 plays a dominant role for $\alpha_{AC} < \alpha_c$. For $\alpha_{AC} > \alpha_c$ we observe a dramatic change in the importance of those diagrams, and we can no longer identify a class of diagrams that provides the major contribution to the self-energy $\Sigma(\tau)$.

The knowledge of a certain class of dominant diagrams can be exploited to develop approximate schemes. Indeed, one can set up a self-consistent scheme thereby summing over an important class of diagrams, including the observed dominant ones. In practice, the procedure can be realized by introducing bold (or dressed) propa-

gators

$$\begin{aligned} \Sigma^{(i-1)}(\mathbf{p}, \omega) &= \int d\omega' \int \frac{d\mathbf{q}}{(2\pi)^3} \\ &\times G^{(i-1)}(\mathbf{p} - \mathbf{q}, \omega - \omega') \mathcal{D}(\mathbf{q}, \omega') \quad (36) \\ G^{(i)}(\mathbf{p}, \omega) &= \frac{1}{G^{0-1}(\mathbf{p}, \omega) - \Sigma^{(i-1)}(\mathbf{p}, \omega)}, \end{aligned}$$

with ω and ω' the imaginary frequencies. The self-energy $\Sigma^{(i-1)}$ and the dressed Green's function $G^{(i)}(\mathbf{p}, \omega)$ are calculated for subsequent values of i , starting from $i = 1$, until $G^{(i)}(\mathbf{p}, \omega)$ is converged. In this way $\Sigma^{(i)}(\mathbf{p}, \omega)$ will contain all diagrams for which the lines of the phonon propagators do not cross.

V. CONCLUSIONS

We have studied the ground-state energies of the BEC polaron and the acoustic polaron, two large polaron systems that can be described by a Fröhlich type of Hamiltonian. When calculating energies for the BEC polaron with the DiagMC and the Feynman variational technique, we encounter similar ultraviolet divergences. For the acoustic polaron, the ultraviolet regularization is achieved by a hard momentum cutoff which is naturally set at the edge of the first Brillouin zone. In this case, the DiagMC and Feynman predictions for the ground-state energies agree within a few percent. The largest deviation between the predictions of both methods, was found at a coupling strength that marks the transition between a quasifree and a self-trapped state. For the BEC polaron, a more involving two-step renormalization procedure is required. The first step is the introduction of a hard momentum cutoff. In line with the results for the acoustic polaron, the DiagMC and Feynman non-renormalized ground-state energies of the BEC polaron which are produced in this step are remarkably similar. Therefore, one can infer that the Feynman variational method reproduces the “exact” DiagMC non-renormalized polaron ground-state energies at a finite momentum cutoff.

In order to obtain the physical, or renormalized, BEC-polaron energies from the non-renormalized ones, an additional procedure is required. Thereby, the contact interaction is renormalized with the aid of the lowest-order correction obtained from the Lippmann-Schwinger equation (34). Despite the fact that the absolute difference between the Feynman and DiagMC BEC-polaron energies remains unaffected by this procedure, the final result for the physical energies displays a large discrepancy.

ACKNOWLEDGMENTS

This work is supported by the Flemish Research Foundation (FWO Vlaanderen) through project numbers G.0119.12N and G.0115.12N. Discussions with

S.N. Klimin and L.A. Pena-Ardila are gratefully acknowledged. The computational resources (Stevin Supercom-

puter Infrastructure) and services used in this work were provided by Ghent University, the Hercules Foundation, and the Flemish Government.

-
- ¹ L. D. Landau, Phys. Z. Sowjetunion **3**, 664 (1933)
 - ² G. Wellein, H. Röder, and H. Fehske, Phys. Rev. B **53**, 9666 (1996)
 - ³ D. J. J. Marchand and M. Berciu, Phys. Rev. B **88**, 060301 (2013)
 - ⁴ H. Fröhlich, Adv. Phys. **3**, 325 (1954)
 - ⁵ F. M. Peeters and J. T. Devreese, Phys. Rev. B **32**, 3515 (1985)
 - ⁶ F. M. Cucchiatti and E. Timmermans, Phys. Rev. Lett. **96**, 210401 (2006)
 - ⁷ K. Sacha and E. Timmermans, Phys. Rev. A **73**, 063604 (2006)
 - ⁸ J. Tempere, W. Casteels, M. K. Oberthaler, S. Knoop, E. Timmermans, and J. T. Devreese, Phys. Rev. B **80**, 184504 (2009)
 - ⁹ V. Shikin and Y. Monarkha, J. Low Temp. Phys. **16**, 193 (1974)
 - ¹⁰ S. A. Jackson and P. M. Platzman, Phys. Rev. B **24**, 499 (1981)
 - ¹¹ G. E. Marques and N. Studart, Phys. Rev. B **39**, 4133 (1989)
 - ¹² G. D. Mahan and J. J. Hopfield, Phys. Rev. Lett. **12**, 241 (1964)
 - ¹³ J. T. Devreese and A. S. Alexandrov, *Advances In Polaron Physics*, Vol. 159 (Springer-Verlag Berlin, 2010)
 - ¹⁴ J. T. Devreese, ArXiv: 1012.4576(2010)
 - ¹⁵ T. D. Lee, F. E. Low, and D. Pines, Phys. Rev. **90**, 297 (1953)
 - ¹⁶ L. D. Landau and S. I. Pekar, Zh. Eksp. Teor. Fiz. **16**, 341 (1946)
 - ¹⁷ S. I. Pekar, Berlin, Akademie Verlag (1951)
 - ¹⁸ R. P. Feynman, Phys. Rev. **97**, 660 (1955)
 - ¹⁹ R. P. Feynman, *Statistical mechanics: A set of lectures* (Addison-Wesley Publ. Co., Reading, MA, 1990)
 - ²⁰ N. V. Prokof'ev and B. V. Svistunov, Phys. Rev. Lett. **81**, 2514 (1998)
 - ²¹ A. S. Mishchenko, N. V. Prokof'ev, A. Sakamoto, and B. V. Svistunov, Phys. Rev. B **62**, 6317 (2000)
 - ²² P. Massignan, M. Zaccanti, and G. M. Bruun, Rep. Prog. Phys. **77**, 034401 (2014)
 - ²³ J. Vlietinck, J. Ryckebusch, and K. Van Houcke, Phys. Rev. B **87**, 115133 (2013)
 - ²⁴ J. Vlietinck, J. Ryckebusch, and K. Van Houcke, Phys. Rev. B **89**, 085119 (2014)
 - ²⁵ M. M. Forbes, A. Gezerlis, K. Hebeler, T. Lesinski, and A. Schwenk, Phys. Rev. C **89**, 041301 (2014)
 - ²⁶ K. K. Thornber, Phys. Rev. B **9**, 3489 (1974)
 - ²⁷ L. Pitaevskii and S. Stringari, *Bose-Einstein Condensation*, 1st ed. (Oxford University Press, 2003)
 - ²⁸ A. Sumi and Y. Toyozawa, J. Phys. Soc. Japan **35**, 137 (1973)
 - ²⁹ R. Fantoni, Phys. Rev. B **86**, 144304 (2012)